Deflashing of automotive formed parts : warpage and tolerance issues

Benrabah, Z.; Debergue, P.; DiRaddo, R.

Publisher's version / Version de l'éditeur:
https://doi.org/10.4271/2006-01-0586
SAE Technical Papers, 2006-04-03

Deflashing of Automotive Formed Parts : Warpage and Tolerance Issues

Z. Benrabah, P. Debergue, R. DiRaddo
Industrial Materials Institute, National Research Council of Canada
75 De Mortagne, Boucherville, Québec, Canada, J4B 6Y4

ABSTRACT

Blow moulding is one of the most important polymer processing method for producing plastic automotive parts. Yet, there are still several problems that affect the overall success of forming these parts. Among them, are thermally induced stresses, relevant shrinkage and part warpage caused by inappropriate solidification conditions. This work presents a finite element model that allows for predicting residual stresses and subsequent deformations that arise during the cooling stage of finished parts. It is expected that the virtual presence of the flash zone has an influence on the development of residual stresses in the numerical model. Deflashing is usually performed immediately after part removal from the mould, therefore, the numerical model is adapted to take this into account. Numerical results obtained with and without flash for a simple part, as well as a complex automotive part, are compared to determine accuracy and limitations of the model.

INTRODUCTION

The forming processes are those where a molten polymeric parison is deformed to take the shape of a mould cavity and subsequently solidifies. Since it is a highly automated process, it is predestined for large-scale manufacturing. During these processes, residual stresses caused by inhomogeneous cooling and relaxation of polymer chains, often result in shrinkage and warpage of the final part.

Shrinkage and warpage are deformation phenomena that occur during the solidification stage of forming operations, both inside the mould and after demoulding [1,2,3]. Tolerance issues are critical in many applications, particularly in the automotive industry, and therefore part deformation due to solidification needs to be controlled and optimized accordingly.

If the polymeric behaviour can be modeled adequately in a simulation, two major advantages can be achieved: first, the influence of different processing variables on the stress profiles can be investigated and consequently adjusted in a way to minimize final residual stresses, second, the knowledge of residual stresses allows the prediction of shrinkage and warpage behaviour of a product. If the dimensional changes of a part can be estimated before a tool is built, the design engineer gets a valuable tool to avoid costly and expensive modifications to the mould.

In this article, a numerical model for the prediction of thermally induced stresses as well as resulting shrinkage and warpage is studied. First, the thermal model used for computing the temperature field of formed parts taking into account polymer crystallization is presented. Then we examine the viscoelastic model used to calculate the large deformations that occur during forming processes. A special emphasis is also placed on the recurrent formulae used for calculating time-dependent residual stresses. The warpage deformation of the part based on a thermo-viscoelastic model is finally derived. Moreover, to show the effect of deflashing on the deformation of final products, two particular cases are presented and analyzed.

THEORETICAL APPROACH

THERMAL MODEL

To evaluate the thermally induced residual stresses developed during the cooling and solidification stages, both inside the mould and after demoulding, a good prediction of the temperature field evolution is first required. Given the inherent low thermal conductivity of plastics, the special geometrical configuration of the formed part i.e. relatively thin compared with their surface area, unilateral cooling is usually assumed to be a one dimensional transient heat conduction problem through the part thickness [4]. Taking into account the effect of heat absorption due to crystallization of the polymer during the cooling stage leads to the following heat balance equation [5]:

$$\rho C_p \frac{dT}{dt} = \frac{\partial}{\partial x}\left(k\frac{\partial T}{\partial x}\right) + \dot{Q}_{Cry} \quad (1)$$

where ρ, C_p and k are the density, specific heat and thermal conductivity of the polymer respectively that may be considered constant or temperature dependent [3], T is the temperature and t is the elapsed time. The $\dot{Q}_{Cry}$ term describes the volumetric heat absorption due to crystallization.

The solution of the balance energy equation (1) depends on the initial temperature values and on the boundary conditions. As initial conditions for the cooling stage, we use the final temperature field provided at the end of the forming stage. It is then assumed that the energy interchange between the outer surface of the part and the surface of the mould before demoulding, and surrounding air after demoulding, occurs by free convection. The energy interchange between the inner surface and cavity air also occurs by lateral free convection. The boundary conditions on the inner and outer surface of the part before demoulding are given as follows:

$$-k\frac{\partial T}{dx} = h_{air}^{part}\cdot\left(T_s^{in} - T_{air}^{in}\right) \quad (2)$$

$$-k\frac{\partial T}{dx} = h_{mould}^{part}\cdot\left(T_s^{out} - T_{mould}\right) \quad (3)$$

After demoulding:

$$-k\frac{\partial T}{dx} = h_{air}^{part}\cdot\left(T_s^{in} - T_{air}^{in}\right) \quad (4)$$

$$-k\frac{\partial T}{dx} = h_{air}^{part}\cdot\left(T_s^{out} - T_{air}^{out}\right) \quad (5)$$

where h_{air}^{part} and h_{mould}^{part} are the convection coefficients between the surface of the part and the air, and the surface of the part and the mould, respectively. They may be considered constant or, more realistically, variable with time and position [2]. T_s^{in} and T_s^{out} are the inner and outer surface temperature of the part, respectively. T_{air} is the air temperature and T_{mould} is the mould temperature.

In equation (1), the crystallization heat absorption $\dot{Q}_{Cry}$ term is given by the following equation:

$$\dot{Q}_{Cry} = \rho\Delta H_{Cry}\frac{\partial\chi}{\partial t} \quad (6)$$

where ΔH_{Cry} is the latent heat of crystallization and χ is the relative degree of crystallinity. According to [4,5,6], the Nakamura model is a well-known model for the prediction of crystallinity during polymer processing. The model is a differential expression that gives the rate of crystallization $\frac{\partial\chi}{\partial t}$ as a function of the temperature T:

$$\frac{\partial\chi}{\partial t} = nK(T)(1-\chi)\left[\ln\left(\frac{1}{1-\chi}\right)\right]^{\frac{(n-1)}{n}} \quad (7)$$

where n is the Avrami exponent and $K(T)$ is the temperature dependent rate constant parameter given by the Hoffman-Lauritzen theory through the following expression:

$$K(T) = K_0\exp\left(-\frac{U}{R(T-T_g+30)} - \frac{C(T+T_m)}{2T^2(T_m-T)}\right) \quad (8)$$

where K_0 is the model constant, U the activation energy, R is the universal gas constant, C is the nucleation exponent, T_g is the glass transition temperature and T_m is the melting temperature.

The set of partial differential equations (1)-(5) describing such a problem is often referred to as the mathematical form or strong form. The differential equations may be either linear or non linear. Consequently, the exact analytical solutions of the heat transfer governing equations can only be obtained for problems in which restrictive simplifying assumptions are made with respect to geometry, material properties and boundary conditions. There is therefore, no option but to turn to numerical solution methods for the analysis of practical problems, where such simplifications are generally not possible.

Based on the Galerkin approximation method and combining the balance equation (1) and the boundary conditions (2)-(5) it is simple to show that the previous thermal problem is reduced to the following compact matrix form [7]:

$$[C(T)]\cdot\{\dot{T}\} + [K(T)]\cdot\{T\} = F(T) \quad (9)$$

in which,

$$\{T\} = \{T_n\}$$

$$C_{IJ} = \int_V\left(N_I\cdot\rho C_p(T)\cdot N_J\right)d\Omega$$

$$K_{IJ} = \int_V\left(\frac{\partial N_I}{\partial x}\cdot k\cdot\frac{\partial N_J}{\partial x}\right)d\Omega + \int_{S_{out}}\left(N_I\cdot h_{mould}^{Part}\cdot N_J\right)ds + \int_{S_{in}}\left(N_I\cdot h_{air}^{Part}\cdot N_J\right)ds + \int_{S_{out}}\left(N_I\cdot h_{air}^{Part}\cdot N_J\right)ds$$

$$F_I = \int_{S_{out}}\left(N_I\cdot h_{mould}^{Part}\cdot T_{mold}\right)ds + \int_{S_{out}}\left(N_I\cdot h_{air}^{Part}\cdot T_{air}^{out}\right)ds + \int_{S_{in}}\left(N_I\cdot h_{air}^{Part}\cdot T_{air}^{in}\right)ds + \int_V\left(N_I\cdot\rho\Delta H_{Cri}\frac{\partial\chi}{\partial t}\right)d\Omega$$

where T_n are the nodal temperatures and N are the element shape functions. For the transient case under consideration, the global capacitance *[C]* and conductance matrices *[K]* are temperature dependent. The non-linearity is due to the temperature dependent thermal conductivity, density, specific heat, and non-

isothermal crystallization kinetics. Since *[C]*, *[K]*, and *{F}* may strongly depend on the unknown temperature, the system of equations (9) may be strongly nonlinear.

Resolution strategy

The numerical solution of equation (9) is obtained by replacing the differential equations with finite difference relationships. Generally, a two-level time scheme is applied, where the solution at a particular time level is directly calculated from the temperature at a previous time level. The following relation is obtained [7]:

$$[C(T_{t+\tau\cdot\Delta t})]\cdot\left\{\frac{T_{t+\Delta t}-T_t}{\Delta t}\right\}+[K(T_{t+\tau\cdot\Delta t})]\cdot\{T_{t+\tau\cdot\Delta t}\}=F(T_{t+\tau\cdot\Delta t}) \qquad (10)$$

Using this algorithm with $\tau = 0$ corresponds to the Explicit Euler Scheme. The discrete set of differential equations becomes:

$$[C(T_t)]\cdot\{T_{t+\Delta t}\}=[[C(T_t)]-\Delta t\cdot[K(T_t)]]\cdot\{T_t\}+\Delta t\cdot F(T_t) \qquad (11)$$

Where the resolution at time $t+\Delta t$ requires the inversion of the capacitance matrix *[C]*. It can be seen from equation (11) that the temperature value at time $t+\Delta t$, $T_{t+\Delta t}$, is directly evaluated from the current values T_t at time t, thereby returning the explicit nature of the algorithm. It was proved that this algorithm is conditionally stable and first order of accuracy. According to the level of non-linearity this scheme seems well adapted to our problem.

FORMING DEFORMATIONS

Based on the principal of stationary potential energy, we know that the total energy Π of a deformable body submitted to external loads tends to a minimum with regards to the displacement, which is expressed as [8]:

$$\delta\Pi=\delta\Pi_{int}+\delta W_{ext}=0 \qquad (12)$$

where $\delta\Pi_{int}$ is the variation of strain energy of the deformable body and δW_{ext} is the variation of the work of external forces. In Lagrangian formulation, the variation of the strain energy can be expressed as a function of the 2nd deviatoric Piola-Kirchoff stress tensor S^d and the conjugated green-Lagrange strain tensor E as follows:

$$\delta\Pi_{int}=\int_{V_0}S_{ij}^{d}\delta E_{ij}dV \qquad (13)$$

where V_0 is the volume of the undeformed body.

The rheological model used to describe the viscoelastic deformations that occur during polymer forming processes i.e. stress(S^d)–strain(E) relationship of equation (13), is the KBK-Z model. This model is well known to adequately represent polymer behaviour at the molten state [9,10,11]. It gives the true stresses σ at time t as a function of the strain history according to:

$$\boldsymbol{\sigma}(t)=-p\mathbf{I}+\frac{1}{1-\theta}\int_{-\infty}^{t}M(t-\tau)h(\mathbf{I}_1,\mathbf{I}_2)\left[\mathbf{C}^{-1}(t,\tau)+\theta\,\mathbf{C}(t,\tau)\right]d\tau \qquad (14)$$

where p is the iso-static pressure, $M(t-\tau)$ is the memory function, $h(I_1,I_2)$ the damping function [12], and $C(t,\tau)$ and $C^{-1}(t,\tau)$ are the Cauchy and Finger strain tensors, respectively [9,10]. The memory function $M(t-\tau)$ is defined by:

$$M(t-\tau)=\sum_k\frac{g_k}{\tau_k}\exp\left(-\frac{t-\tau}{\tau_k}\right) \qquad (15)$$

where g_k, τ_k are the materials relaxation modulii and times respectively. The WLF equation incorporates the thermal dependence of the material properties through the following relationship, the shift factor a_T being subsequently applied to the relaxation times τ_k:

$$\ln(a_T)=-\frac{C_1(T-T_{ref})}{C_2+T-T_{ref}} \qquad (16)$$

where T is the temperature, obtained from the previously presented thermal model, C_1 and C_2 are material constants and T_{ref} is the reference temperature. Numerical results obtained from the forming processes (mainly thickness and temperature distribution) are the base for the subsequent calculation of shrinkage and warpage deformations.

SRINKAGE AND WARPAGE DEFORMATIONS

Once the polymeric parison melt is inflated inside the cavity, it rapidly cools down and solidifies until it has enough strength to be taken out of the mould for additional cooling in ambient air. While in the mould, thermal stresses start developing due to non-uniform wall thickness and temperature profiles. After demoulding, formed parts undergo shrinkage and warpage caused by accumulated thermal stresses, additional mechanical stresses and temperature evolution.

Resolution strategy

After the computation of thermal stresses during in-mould cooling, a finite element analysis of the demoulded part subject to equilibrium loads will provide the corresponding displacements according to an appropriate thermo-viscoelastic constitutive equation. The computed displacements are in turn interpreted in terms of shrinkage deformations, due to the change in density during cooling and warpage distortions. These computed displacements are then used to display the deformed shape of the part.

The residual stresses in the material at time step *n+1* are obtained from the stresses and deformations at time step *n* according to:

$$\sigma_{ij}^{n+1} = \sum_k \bar{g}_k \sigma_{ij}^{r,n+1} \quad (17)$$

$$\sigma_{ij}^{r,n+1} = e^{-\Delta t/\bar{\tau}_k} \sigma_{ij}^{r,n} + \left\{[H]\Delta\varepsilon_{ij} - \sigma_{ij}^{th}\right\}\frac{\bar{\tau}_k}{\Delta t}\left[1 - e^{-\Delta t/\bar{\tau}_k}\right] \quad (18)$$

where *[H]* is the matrix containing the elastic coefficients of the material, ε represents the deformation tensor (small displacement theory), $\bar{g}_k$ and $\bar{\tau}_k$ are the spectra of elastic modulii and relaxation times at solid state, respectively. σ_{ij}^{th} are the thermal stresses defined by:

$$\sigma_{ij}^{th} = \frac{-E(t)}{3(1-\nu)}\frac{v(t)-v(t_0)}{v(t_0)}\delta_{ij} \quad (19)$$

where $v(t)$ is the material's specific volume, which comes from PVT data, and $\frac{v(t)-v(t_0)}{v(t_0)}$ is the material's volumetric dilatation. The modulus $E(t)$ is given by a Maxwell-Weichert viscoelastic model with six relaxation times:

$$E(t) = \sum_{i=1}^{6} E_i e^{-t/\tau_i} \quad (20)$$

Finally, the small displacement theory is linear and has been widely used to model the solidification phenomenon of polymer parts [13,14]. Moreover, it has been proven that the extension to a large displacement approach is not the main contribution to the validity of the model [1,3]. Therefore, using the small displacement theory, the following equilibrium equation is solved once the part exits the mould:

$$[K_s]\{\Delta u\}\frac{\bar{\tau}_k}{\Delta t}\left(1 - e^{-\Delta t/\bar{\tau}_k}\right) = K^{th}\left\{F^{th}\right\}\frac{\bar{\tau}_k}{\Delta t}\left(1 - e^{-\Delta t/\bar{\tau}_k}\right) - \left\{F_\sigma^{r,n}\right\}e^{-\Delta t/\bar{\tau}_k} \quad (21)$$

where F_σ and F^{th} are the forces due to accumulated and thermal stresses, respectively. $[K_s]$ is the stiffness matrix and *u* represents the nodal part displacement.

VALIDATION CASE

Deflashing usually occurs immediately after part removal from the mould. In an effort to be as close to the actual process as possible, the objective here is to simulate deflashing and study its effect on the predictions of residual stresses and warpage.

The detection of the flash area in the numerical model is performed using a homemade algorithm that compares the predicted formed part to the actual finished part. Elements in the cavity are kept while those outside the cavity, using a given tolerance, are removed. A numerical analysis of a simple part is presented first to assess the validity of the approach. Warpage predictions of demoulded parts obtained while keeping the flash area are compared to those obtained when removing the flash. It has already been seen that the influence of the part positioning while out of mould cooling, and thus the type of boundary conditions applied, is important [1,3]. It is then suspected that the presence of extra material (thick and hot) in the flash area will affect the overall boundary conditions applied on the part and in consequence will also affect the final warpage distortions.

The part studied here is a gas container as shown in Figure 1. The simulations consider the parison extrusion, clamping, inflation and solidification. The cooling process is performed in two steps, the first one being in the mould where the flash is present but the part cannot freely deform due to boundary conditions of the mould, and the second one being outside the mould where in one case the flash is present and in the second case the flash is removed. Once the part is removed from the mould cavities, it is then free to deform. The material considered for the study is a typical HDPE blow-moulding grade. It is characterized using standard tests for specific heat, density, thermal conductivity and relaxation spectrum at molten and solid states, to cover the entire temperature range during solidification. The thermal expansion coefficients, which have to be accurately determined to better simulate warpage, are derived from material PVT data.

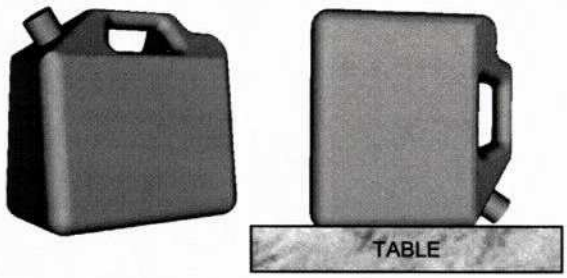

Figure 1. Gas container blow moulded part. Position while out of mould cooling.

NUMERICAL COMPARISONS

Considering the position of the part during out of mould cooling (Figure 1), appropriate boundary conditions are applied on the numerical model through proper nodal point fixings. Figure 2 shows numerical results obtained with and without flash after 42 sec. of in mould cooling, and subsequent out of mould cooling at ambient temperature and natural convection.

It appears from Figure 2 that the deflashing process has been successful and that the final shape of the warped part obtained with and without flash is different, which was expected. Moreover, looking at the thickness distribution, represented by the color scale in Figure 2, we see that even though both predictions present the same thickness distribution, they don't deform the same

way. Hence, as for the thickness profile, deflashing also plays an important role in the final product shape.

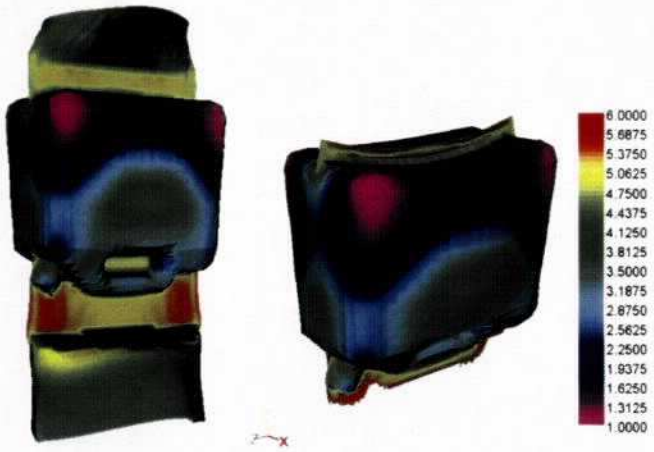

Figure 2. Numerical thickness results obtained with (left) and without flash (right).

Shrinkage and warpage deformations could be quite complex, therefore to help compare the numerical results, the amplitude of the deformation will be represented in this section as a displacement in the 3 coordinate directions, x (transverse), y (vertical) and z (longitudinal). The amplitude of the displacement in the transverse (x) direction is presented in Figures 3 and 4.

Figure 3. Comparison of the transverse displacement amplitude (x direction) obtained with (left) and without flash (right).

Figure 3 shows that the transverse deformation is higher for the part without flash. Also it can be seen that the overall warpage with respect to the ideal part geometry, shown in grey on the figures, is higher as well. Figure 4 shows the displacement evolution along the vertical axis.

A difference of 3 to 4mm in amplitude is observed mainly in the center of the part. This could be more easily explained by looking at the displacement in the vertical (y) direction, that is the direction of the flash in Figures 5 and 6.

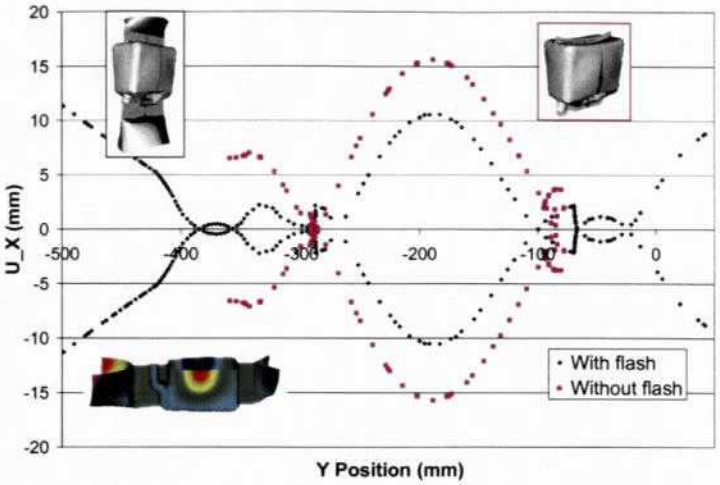

Figure 4. Evolution of the transverse displacement amplitude along the vertical axis obtained with and without flash.

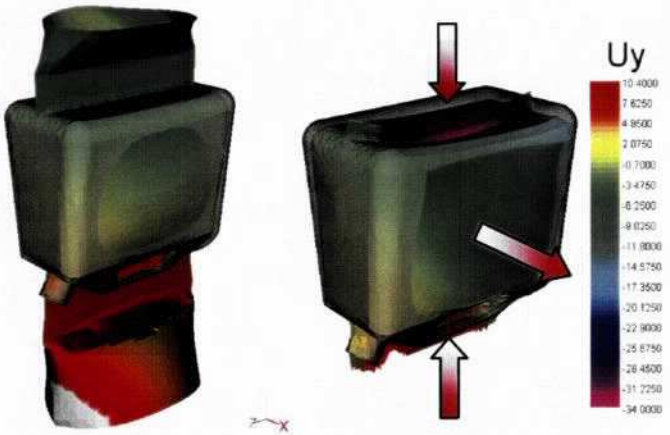

Figure 5. Comparison of the vertical displacement amplitude (y direction) obtained with (left) and without flash (right).

Figure 5 shows that the vertical displacement is a lot higher for the simulation without flash compared to the simulation with flash. Particularly on the bottom of the part where the part adopts a concave shape for the simulation without flash compared to a more straight shape for the simulation with flash. Therefore, the deformation that occurs in the flash direction is directly related to the deflashing process. The increase in the displacement amplitude observed previously in the transverse (x) direction (Figures 3 and 4), is a consequence of the changes occurring in the vertical direction, represented by the arrows in Figure 5.

Figure 6 presents the outline of the two geometries in the YZ plane (front view) and gives a nice overview of the difference between the two simulations. From these results, we can say that the flash area, which is quite important in this validation case, plays a boundary condition role that prevents certain deformations to occur. Once the flash is removed, the part tends to deform more freely.

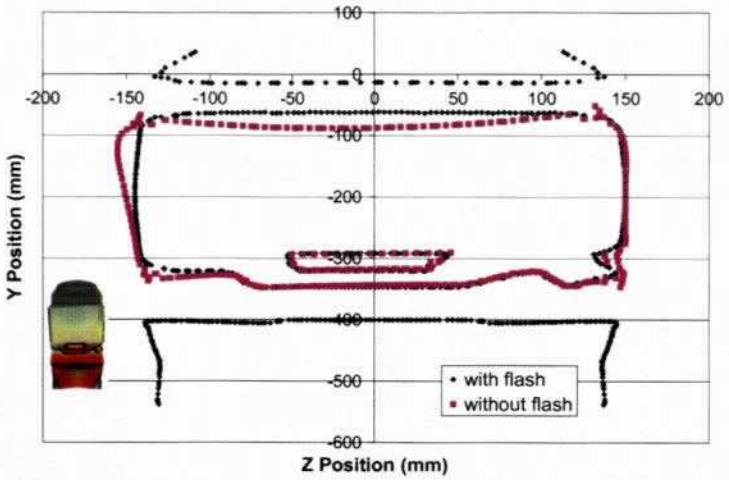

Figure 6. Comparison of the geometries outline in the YZ plane (front view) obtained with and without flash.

AUTOMOTIVE PART

Tolerance issues are critical in automotive applications and therefore part deformation due to solidification needs to be controlled and optimized accordingly. Formed parts can experience a wide range of deformations depending on the cooling conditions that the part is subjected to. Besides the cooling conditions, it is important that the numerical simulation takes into account the deflashing process that usually occurs immediately after demoulding.

The second part studied is a blow-moulded automotive fuel tank (Figure 7). It is more complex and larger than the gas container presented in the previous section. Fuel tank walls are usually made of layers of different materials (multilayer blow moulding) but as it is not the subject of the present study, only a monolayer HDPE blow-moulding grade is considered in this study. Also, in order to minimize cycle time, out of mould cooling conditions may be quite complex for such products. As there are no experimental data to refer to in the present case, we'll consider a part that is fixed only at some nodal point as if it is laid flat on the floor on one side (Figure 7).

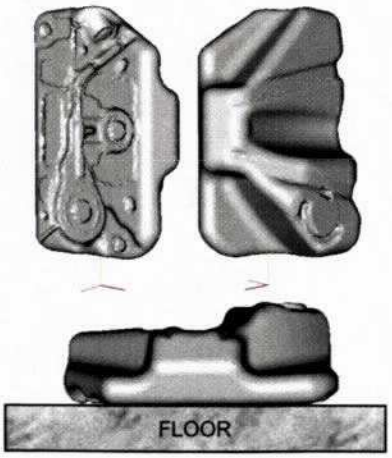

Figure 7. Blow moulded fuel tank. Position while out of mould cooling.

NUMERICAL COMPARISONS

Our goal here is once again to numerically validate the warpage module and evaluate its ability to take into account deflashing. Hence, the focus is put on comparing warpage predictions obtained with and without flash. To help compare the results, the amplitude of the combined shrinkage/warpage deformation is also represented here as a displacement in the 3 coordinate directions, x (longitudinal), y (vertical), and z (transverse). Figure 8 shows the simulation results obtained with and without flash, the color scale represents the displacement amplitude in the x (longitudinal) direction.

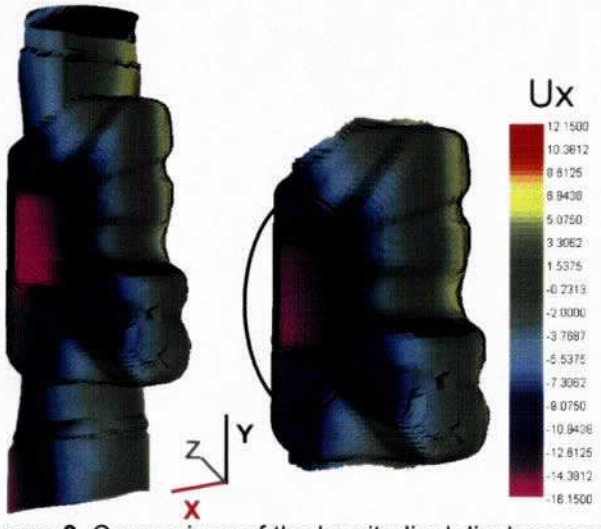

Figure 8. Comparison of the longitudinal displacement amplitude (x direction) obtained with (left) and without flash (right).

Once again, the technique of removing the flash area is successful, however, in this case, we don't see a clear difference between the two predictions. A slight variation is observed on one extremity of the part and is better represented in Figure 9.

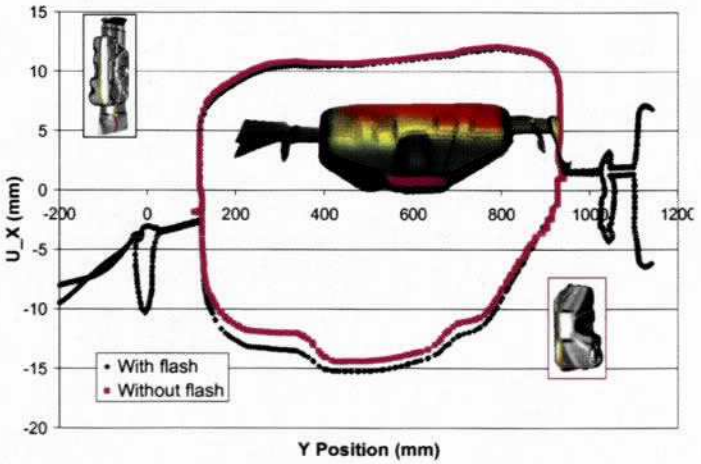

Figure 9. Evolution of the longitudinal displacement amplitude along the vertical axis obtained with and without flash.

Figure 9 shows that the amplitude of deformation in the longitudinal direction is 1 to 2 mm higher for the part with flash. This is quite small compared to the dimensions of the part and very difficult to spot any differences between the deformed part and the ideal geometry. It is important at this point to look at the other directions of deformation, such as the vertical direction (y). In the previous section it was shown that the direction most influenced by the removal of flash was the vertical one (i.e. y –coordinate). Figure 10 presents the amplitude of deformations in the vertical direction (y) for the two numerical predictions.

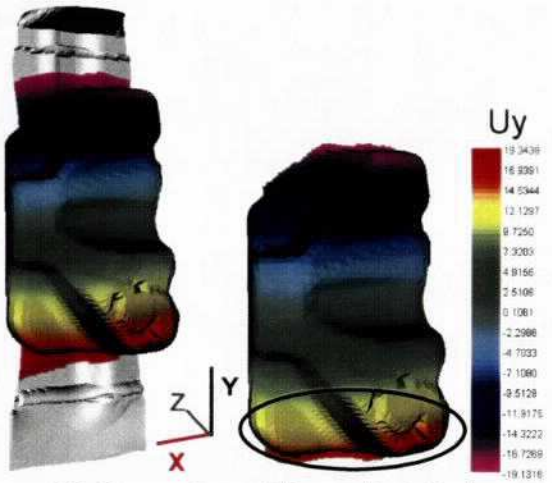

Figure 10. Comparison of the vertical displacement amplitude (y direction) obtained with (left) and without flash (right).

While the largest displacement amplitude is located in the flash area in the case of the simulation with flash, the deformation of the two cavities is very similar. The main difference is observed at the lowest extremity of the part. This difference is illustrated on Figure 11 that presents the displacement amplitude obtained in the vertical (y) direction as a function of the transverse (z) direction.

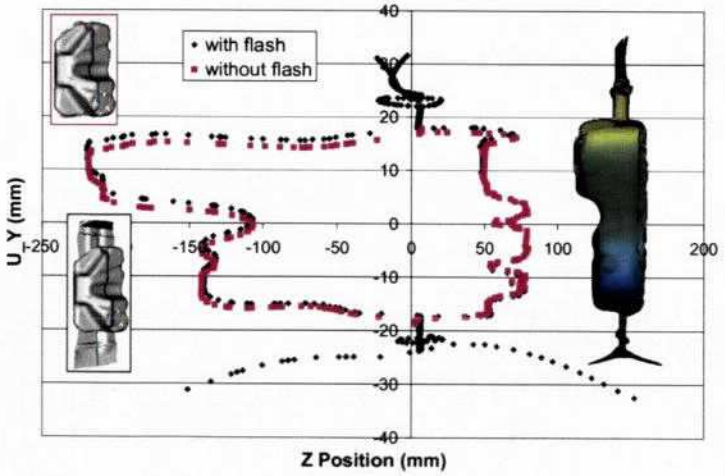

Figure 11. Evolution of the vertical displacement amplitude along the transverse axis obtained with and without flash.

A difference of 1 to 2 mm between the two predictions is observed which is again very small compared to the overall dimensions of the part. The same observations are made for the displacement amplitude in the transverse (z) direction illustrated in Figure 12.

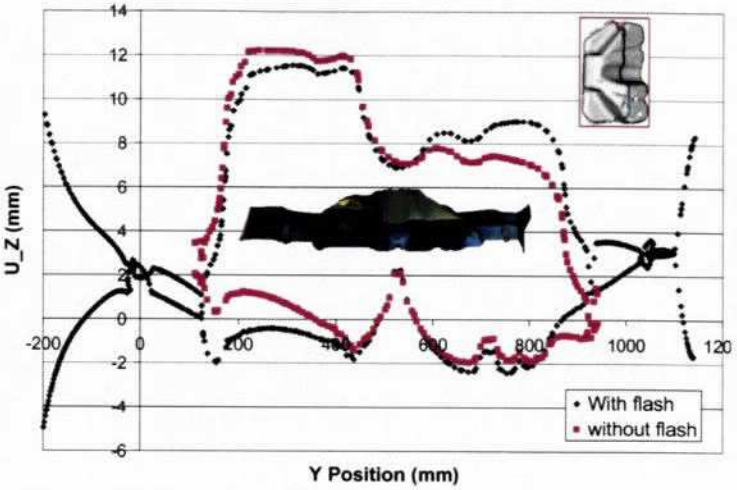

Figure 12. Evolution of the transverse displacement amplitude along the vertical axis obtained with and without flash.

Unlike the displacement amplitude in the longitudinal and vertical directions, the transverse direction is highly non-symmetric. This could be due to the location of the fixed nodal points representing the boundary conditions. As previously demonstrated [1,3], choosing other boundary conditions may affect the overall shrinkage/warpage deformation of the part. Despite the small change in displacement amplitude, it is observed in Figure 12 that the removal of the flash area has an impact on the way the part is deforming during solidification; i.e. there is a rotation effect around the fixed nodal points when the flash is removed that does not appear if the flash is kept. The presence of flash seems to prevent the part to deform in certain ways. This reinforces the fact that the flash area acts as a boundary condition and consequently affects the part warpage.

CONCLUSION

In this work, the effect of deflashing on the solidification deformation of formed polymer parts is investigated. The focus is set on warpage prediction, comparing numerical simulations obtained with and without flash. The thermal and viscoelastic material models, together with the proposed finite element formulations, are detailed. A simple and a complex part are used for the study.

The simple part (gas container) shows a high sensitivity to the presence of the flash. The numerical predictions are shown to be quite different for the part with flash compared to the one without flash. On the contrary, the automotive part studied (fuel tank) is a lot less sensitive to deflashing. However, in both cases the flash area seemed to act like a type of boundary condition, hence affecting the deformation of the part when it is cooled. Therefore, when the part is removed from the mould, the

way it is handled, and whether it is deflashed or not, may lead to various warped shapes. It is thus critical that the simulation takes into account precisely the way the part is handled and held during its cooling phase. Further experimental validations are still necessary to assess the validity of the proposed approach and conclusions.

ACKNOWLEDGMENT

The authors would like to acknowledge the contribution of the members of the SIGBLOW-SIGFORM groups.

REFERENCES

1. Debergue P., Massé, H., Thibault, F., Dirrado, R., J. of Materials and Manufacturing, 112 (5), 2004.
2. Massé H., Debergue P., Diraddo R., ANTEC 2004 Congress, Chicago.
3. Debergue P., Massé, H., Thibault, F., Dirrado, R., ESAFORM 2003 Congress, Salerno (Italy).
4. Dirrado, R, Plast. Rubber Compos. Process. Appl., 24 (4), 189-196, 1995.
5. Glomsaker, T., Larsen, A., Andreassen, E., Polymer Engineering and Science, 45 (7), 945-952, 2005.
6. Patel, R.M., Sprueill, J.E., Polymer Engineering and Science, 31 (10), 730-738, 1991.R.W. Lewis, K.
7. Morgan, H.R. Thomas, K. N. Seetharamu, The Finite Element Heat and Mass Transfer Analysis, J. Wiley & Sons (1996)
8. Bonet, J., Wood R.D., Nonlinear Continuum Mechanics for Finite Element Analysis, Cambridge University Press, (1997).
9. Laroche D., Pecora L., DiRaddo R., Puempel A, Savoni L. SPE ANTEC Tech. Papers, 1998.
10. Laroche D., Kabanemi K., Pecora L., DiRaddo R., Polym. Eng. Sci., 39 (7), 1999.
11. Ferry, J.D., Viscoelastic Properties of Polymers, J. Wiley & Sons (1980)
12. Papanastasiou A. C., Scriven L. E., Macosko C. W. J. Rheol. 27, 387-410. 1983.
13. K.K. Kabanemi, M.J. Crochet, Int. Polymer Processing, 1992
14. K.K. Kabanemi, H. Vaillancourt, H. Wang, G. Salloum, Polym. Eng. Sci., 38 (1), 1998.